TOPICAL REVIEW — Topological insulator

Elastic scattering of surface states on three-dimensional topological insulators*

Wang Jing(王 靖)[a)b)], and Zhu Bang-Fen(朱邦芬)[a)c)†]

[a)] State Key Laboratory of Low-Dimensional Quantum Physics, and Department of Physics, Tsinghua University, Beijing 100084, China
[b)] Department of Physics, McCullough Building, Stanford University, Stanford, California 94305-4045, USA
[c)] Institute of Advanced Study, Tsinghua University, Beijing 100084, China

(Received 13 May 2013)

Topological insulators as a new type of quantum matter materials are characterized by a full insulating gap in the bulk and gapless edge/surface states protected by the time-reversal symmetry. We propose that the interference patterns caused by the elastic scattering of defects or impurities are dominated by the surface states at the extremal points on the constant energy contour. Within such a formalism, we summarize our recent theoretical investigations on the elastic scattering of topological surface states by various imperfections, including non-magnetic impurities, magnetic impurities, step edges, and various other defects, in comparison with the recent related experiments in typical topological materials such as BiSb alloys, Bi_2Te_3, and Bi_2Se_3 crystals.

Keywords: topological insulator, surface state, scattering by imperfection, scanning tunneling microscope

PACS: 73.20.–r, 68.37.Ef, 73.43.Cd, 72.10.Fk **DOI:** 10.1088/1674-1056/22/6/067301

1. Introduction

The discovery of topological insulators (TIs) has attracted a great deal of attention.[1,2] A three-dimensional (3D) TI has a time-reversal invariant band structure with a nontrivial topological order, which possesses an energy gap in the bulk and gapless metallic states on the surface. The surface band consist of an odd number of Dirac cones with unconventional spin texture in the surface Brillouin zone. One of the intriguing properties of such spin-textured surface states (SSs) is their insensitivity to spin-independent scattering, which is protected from backscattering by the time-reversal symmetry (TRS). Exotic excitations such as Majorana fermions,[3] magnetic monopole,[4] and dynamical axion field[5] are predicted to exist as the results of topological SSs.

Soon after the theoretical prediction,[6] $Bi_{1-x}Sb_x$ alloy with composition x ranged from 0.07 to 0.22 was found to be a TI with five Dirac cones by the angle-resolved photoemission spectroscopy (ARPES).[7] ARPES measurements observed topologically nontrivial SSs, and the spin-resolved ARPES measurements reported the helical spin texture of the massless Dirac fermions in the system.[8] However, the SSs in $Bi_{1-x}Sb_x$ are rather complicated, which can hardly be described by a simple model Hamiltonian. Subsequently, a family of binary compounds, Bi_2Se_3, Bi_2Te_3, and Sb_2Te_3, was discovered and investigated as the second generation of TIs.[9–12] Among them, the Bi_2Se_3 contains only a single Dirac cone within a gap as large as 300 meV, and as the "hydrogen atom" of TIs is easier to study. The helical spin texture of SSs in Bi_2Se_3 is observed to be left-handed.[11] Intensive investigations indicate that the direct backscattering between the time-reversal pair of helicity states with opposite momenta and spins is prohibited, and the Anderson localization will not occur in this two-dimensional (2D) helical liquid.

In addition to the ARPES, the low-temperature scanning tunneling spectroscopy (STS) as well as microscope (STM) is another important probe in the TI research, which provides a direct way to study the SSs through measuring the local density of states (LDOS) in the vicinity of various imperfections. Due to the elastic scattering by impurities, the incoming surface wave with a wavevector $\boldsymbol{k}^{\mathrm{i}}$ must be scattered into an outgoing one with $\boldsymbol{k}^{\mathrm{f}}$ on the same constant energy contour (CEC). The quantum interference between the incoming and the outgoing waves gives rise to the standing wave oscillation with wavevector $\boldsymbol{q} = \boldsymbol{k}^{\mathrm{f}} - \boldsymbol{k}^{\mathrm{i}}$, which is often referred as the characteristic scattering wavevector, or the transferred momentum. Energy-resolved Fourier transform STS (FT-STS) can be used to obtain the scattering wavevectors of modulations in the LDOS and detailed information on the symmetry as well as the physics of scattering processes for the SS electrons.[13] This technique has been proved valuable in studying the SSs on noble metals[14] and semiconductor surfaces,[15] and even on

*Project supported by the Basic Research Program of China (Grant No. 2011CB921901) and the National Natural Science Foundation of China (Grant No. 11074143).

†Corresponding author. E-mail: bfz@mail.tsinghua.edu.cn

© 2013 Chinese Physical Society and IOP Publishing Ltd

the pairing symmetry of the high-T_c superconductors[16] and graphene.[17] The absence of backscattering is a specular manifestation of the topological nature of the SSs. Different from the edge states in 2D TIs, in which the forbidden backscattering means the annihilation of all types of elastic scatterings by the spin-independent potentials, the SSs in 3D TIs will experience single-particle elastic scattering associated with all scattering angles except for 180° backscattering. Thus investigating the quasiparticle interference (QPI) caused by scattering off impurities and defects on the TI surfaces and revealing the topological nature of the SSs through the FT-STS are interesting and useful, in particular based on the combination of theoretical and experimental investigations.

The QPI patterns induced by non-magnetic impurities on the surfaces of Bi_xSb_{1-x},[18] Bi_2Te_3,[19] and Bi_2Se_3,[20] together with subsequent theoretical analyses,[21–26] do demonstrate the absence of backscattering for the topological SSs. Meanwhile, the LDOS oscillations of the SSs near step edges on Bi_2Te_3 show a power-law decay with index $-3/2$, $-1/2$, and -1 for the SSs in different energy ranges,[26,27] while in Bi_2Se_3 the decay index is fixed to be $-3/2$,[26,28] compared to $-1/2$ for the 2D electron system (2DES).[14] The faster decay of the QPI pattern is believed to result from the suppression of backscattering in TIs. For magnetic impurities on Bi_2Te_3 which break the TRS, although the TR violating scattering wavevectors have been reported,[29] it is still controversial whether the direct backscattering between the time-reversal pair is responsible for the unusual sensitivity to the magnetic scattering.[20]

So far comprehensive STM and ARPES investigations have demonstrated the topological properties of SSs; however, a general picture about the scattering properties and interaction processes of SSs, including the elastic scattering by impurities and defects between SSs, and quasi-elastic SS-longitudinal acoustic (LA) phonon interaction, remains elusive. For example, the QPI patterns on the surface of various TI systems, with a lot of physical factors involved, are not easy to interpret, particularly when the quality of TI samples and the warping effect of the Dirac cone are taken into account.[12,30] Here, the warping effect includes not only the anisotropic band dispersion of the SSs, but also the anisotropic coupling between the surface and bulk bands. In this article, we will give a comprehensive review on the elastic scattering of SSs in various TI systems. The SS–LA phonon quasi-elastic scattering plays an important role in the transport of SSs,[31] but does not affect the QPI pattern significantly, so it will not be discussed in this article. With the recent experimental results, we present a general formalism to account for the complex QPI on the TI surface. We propose that the interference patterns are dominated by the SSs at the extremal points on the CEC. By applying this theory to Bi_2Te_3 with the strong warping effect, we show that, when tuning the bias voltage, for scattering off a non-magnetic impurity, the QPI wavevector depends on the shape of the Fermi surface sensitively, which varies from conical to $\bar{\Gamma}$–$\bar{K}$ and finally to $\bar{\Gamma}$–$\bar{M}$, as the CEC changes from circle to hexagon and finally to snowflake. And the decay index off a step edge also critically depends on the energy of SSs, varying from $-3/2$ to $-1/2$ and finally to -1 as energy increases. As for the TIs with a nearly isotropic Dirac cone, such as Bi_2Se_3,[32] according to our theory the decay index is simply $-3/2$. For the scattering off a magnetic impurity, the direct backscattering is allowed due to the TRS breaking. However, we will show that such a backscattering between time-reversal pairs in the presence of TRS breaking can be hardly singled out in LDOS by STM. Therefore, the QPI pattern of magnetic impurity is still similar to that of non-magnetic impurity.

The organization of this paper is as follows. Section 2 describes the general theory for the QPI of 2D SSs. There we focus on the Bi_2Se_3 family, as their SSs can be described by a simple Hamiltonian. Section 3 is devoted to the standing wave due to step edge scattering compared to experiments. Section 4 describes the QPI pattern by scattering off the non-magnetic impurity in combination with the related experiments. Section 5 describes the scattering of SSs by the magnetic impurity. Section 6 summarizes the experimental studies on the scattering off surface fluctuation and one-dimensional buckling. Section 7 concludes this paper with a short summary and discussion.

2. General theory

The topological SSs on Bi_2Te_3 and Bi_2Se_3 have a single Dirac cone near $\bar{\Gamma}$ point in the surface Brillouin zone of each surface. The effective model describing such topological SSs reads[30]

$$\mathscr{H}_0(\boldsymbol{k}) = v(\sigma_x k_y - \sigma_y k_x) + \frac{\lambda}{2}\left(k_+^3 + k_-^3\right)\sigma_z, \tag{1}$$

where $\hbar \equiv 1$, $k_\pm \equiv k_y \pm \mathrm{i}k_x$, v is the Dirac velocity, λ is the warping parameter, and σ_i $(i = x, y, z)$ are the Pauli matrices acting on the spin space. For simplicity, we ignore the particle–hole asymmetry here as it affects the shape of the Fermi surface slightly. The surface band dispersion is

$$\varepsilon_\pm(k_x, k_y) = \pm\sqrt{v^2k^2 + \lambda^2k^6\sin^2(3\theta)}, \tag{2}$$

where $\varepsilon_\pm$ denote respectively the upper and the lower energy bands touching at the Dirac point, and $\boldsymbol{k} \equiv (k, \theta)$ with θ being the angle between wave vector $\boldsymbol{k}$ and the k_x axis ($\bar{\Gamma}$–$\bar{M}$). Defining the characteristic energy $\varepsilon^* \equiv v\sqrt{v/\lambda}$ and length $d \equiv \sqrt{\lambda/v}$, we plot in Fig. 1 a set of CECs of the upper band in

momentum space with no free parameters for both Bi_2Se_3 and Bi_2Te_3. For Bi_2Se_3, $\lambda = 128$ eV·Å^3 and $\varepsilon^* = 0.52$ eV,[9,32] so the CEC is nearly isotropic from 0 to $0.42\varepsilon^*$ (0.22 eV). As shown in Fig. 1, when the Fermi energy increases, the shape of the CEC evolves from a circle ($E = 0.31\varepsilon^*$), more hexagon-like ($E = 0.55\varepsilon^*$), hexagon ($E = 0.7\varepsilon^*$), to concave hexagon ($E = 1.0\varepsilon^*$). For Bi_2Te_3, $\lambda = 250$ eV·Å^3 and $\varepsilon^* = 0.23$ eV,[12] so the warping effect is stronger. As shown in Fig. 1, when the Fermi energy increases, the shape of the CEC evolves from a hexagon ($E = 0.7\varepsilon^*$), concave hexagon ($E = 1.46\varepsilon^*$), more hexagram-like ($E = 1.91\varepsilon^*$), to the six-pointed shape of snowflake ($E = 2.4\varepsilon^*$). The evolution of the Fermi surface with respect to energy agrees well with the ARPES results.[12,32] As we shall see, such changes in the shape of the Fermi surface have drastic effects on the QPI around an impurity.

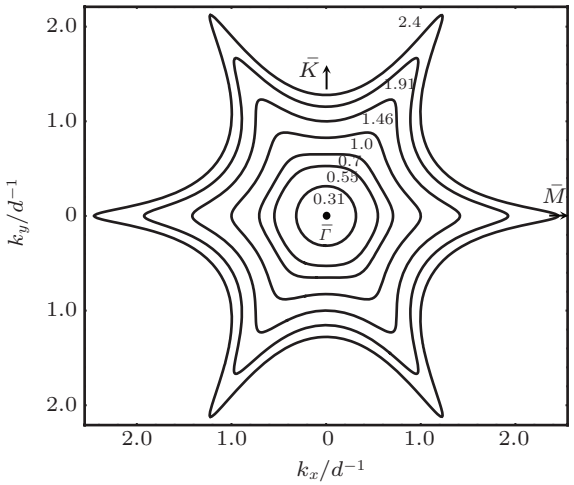


Fig. 1. Unified contours of constant energy and the evolution of the Fermi surface of topological SSs in both Bi_2Se_3 and Bi_2Te_3, where k_x and k_y are in units of $\sqrt{v/\lambda}$, and the energy is in units of ε^*. The contours with Bi_2Se_3 parameters and ε^* taken from 0.3 to 0.7 are suitable for Bi_2Se_3, and those with Bi_2Te_3 parameters and ε^* from 0.7 to 1.91 are for Bi_2Te_3.

We study the quasiparticle scattering problem within the T-matrix approach. For a single non-magnetic or magnetic impurity located at the origin ($\boldsymbol{r} = 0$) on the surface with the coupling

$$\mathscr{H}_1 = V\delta(\boldsymbol{r})\sigma^\mu, \tag{3}$$

where $\sigma^\mu = 1_{2\times 2}$ ($\mu = 0$) denotes the non-magnetic impurity, and the Pauli matrix σ^μ ($\mu = x, y, z$) denotes the magnetic impurity, the LDOS can be expressed as

$$\begin{aligned}\rho(\boldsymbol{r},\omega) &= -\frac{1}{\pi}\mathrm{Im}\left[\mathrm{Tr}\left[G(\boldsymbol{r},\boldsymbol{r},\omega)\right]\right] \\ &= \rho_0(\boldsymbol{r},\omega) + \delta\rho(\boldsymbol{r},\omega),\end{aligned} \tag{4}$$

where $\rho_0(\boldsymbol{r},\omega)$ is the LDOS of the unperturbed system ($V = 0$), and $\delta\rho(\boldsymbol{r},\omega)$ is the deviation of the LDOS induced by the perturbation $\mathscr{H}_1$.

Let the unperturbed surface Green's function be G_0, the perturbed Green's function can be expressed as

$$G(\boldsymbol{r},\boldsymbol{r}',\omega) = G_0(\boldsymbol{r}-\boldsymbol{r}',\omega) + G_0(\boldsymbol{r},\omega)T(\omega)G_0(-\boldsymbol{r}',\omega), \tag{5}$$

with

$$G_0(\boldsymbol{r},\omega) = \int^{\Lambda} \frac{\mathrm{d}^2k}{(2\pi)^2}\,\mathrm{e}^{\mathrm{i}\boldsymbol{k}\cdot\boldsymbol{r}}G_0(\boldsymbol{k},\omega), \tag{6}$$

$$G_0(\boldsymbol{k},\omega) = \left[\omega + \mathrm{i}\eta - \mathscr{H}_0(\boldsymbol{k})\right]^{-1}, \tag{7}$$

where Λ is the energy cutoff when integrating over momentum, and T is given by

$$T(\omega) = V\sigma^\mu\left[1 - G_0(\omega)V\sigma^\mu\right]^{-1}. \tag{8}$$

Here we assume a translation symmetry in the unperturbed system and a momentum-independent scattering potential. The spatial modulation of the LDOS is induced by $\mathscr{H}_1$ in the vicinity of impurities. To resolve the wave vector of the modulation of interference, it is convenient to calculate the Fourier-transformed LDOS

$$\delta\rho(\boldsymbol{q},\omega) = \int \mathrm{d}^2r\,\mathrm{e}^{-\mathrm{i}\boldsymbol{q}\cdot\boldsymbol{r}}\delta\rho(\boldsymbol{r},\omega). \tag{9}$$

From the real-space LDOS, one can get the power-law decay as a function of the distance away from the impurity center $\delta\rho(\boldsymbol{r},\omega) \propto 1/r^\alpha$. While from the q-space LDOS, one can get the allowed wave vector $\boldsymbol{q}$ and the relative intensities for various scattering processes experienced by the SS electrons. Both the real-space and q-space information can be obtained by STM.

For the case of scattering by a step edge, the scattering potential is taken as $V\delta(x)$. It is straightforward to compute the LDOS by the standard procedure described above. However, without loss of generality, it is more convenient to treat the scattering problem by using an analogy of the elementary scattering problem with a barrier potential, either in 1D (step-edge) or 2D with rotational symmetry (magnetic or non-magnetic impurity), which is directly based on the wave function point of view. We will discuss the formalism in Subsections 3.1 and 4.1, respectively.

3. Scattering by step-edge

3.1. Theory

Let us first consider the scattering of SSs by a step edge. The step on a surface along a crystallographic axis in principle reduces the interference to a 1D problem. The step edge in a 2D conventional Fermi gas is known to give rise to the Friedel oscillation at a fixed energy in the LDOS.[14] Since the step edge scattering is a type of elastic scattering, the incoming SS with wave vector $\boldsymbol{k}^{\mathrm{i}}$ and the outgoing one with $\boldsymbol{k}^{\mathrm{f}}$ are on the

same CEC. Assuming a step edge along the y direction, the k_y component of the wave vectors should be conserved in the scattering process, i.e. $k_y^{\rm i} = k_y^{\rm f} \equiv k_y$. The interference between the incoming and the outgoing waves gives rise to the standing wave oscillation in the x direction. The total LDOS is the sum of contributions from all these oscillations from the SSs on a CEC. For a given energy E, we can integrate over k_y on the entire CEC and express the LDOS explicitly as

$$\delta\rho(E,x) = {\rm Re}\left[\oint_E \frac{2r_{\rm c}}{1+|r_{\rm c}|^2}\xi_i^{\dagger}\xi_{\rm f}\,{\rm e}^{{\rm i}(k_x^{\rm f}-k_x^{\rm i})x}{\rm d}k_y\right], \quad (10)$$

where $r_{\rm c}$ is the reflection coefficient of the potential barrier of the step edge, and ξ denotes the spin wave function of the SS of the form $\xi\,{\rm e}^{{\rm i}k_x x+{\rm i}k_y y}$.

A pair of states $\boldsymbol{k}^{\rm i}$ and $\boldsymbol{k}^{\rm f}$ scattered by the step along the y direction results in a standing wave with the spatial period of $2\pi/(k_x^{\rm f}-k_x^{\rm i}) \equiv 2\pi/\Delta k_x$. Since the oscillation period is different for different k_y, a large number of scattering pairs will interfere destructively, and only the pair whose period is stationary with respect to a small variation in k_y may make the dominant contribution to the LDOS oscillations. Such a pair of points [$(k_{x0}^{\rm i},k_{y0})$ and $(k_{x0}^{\rm f},k_{y0})$] on the CEC is called the pair of extremal points (EPs),[33] which satisfies

$$\partial\Delta k_x/\partial k_y|_{k_{y0}} = \partial(k_x^{\rm f}-k_x^{\rm i})/\partial k_y|_{k_{y0}} = 0.$$

Here the characteristic scattering wavevector Δk_{x0} critically depends on the geometry of the CEC. Other standing waves will cancel at large x because of the mutual interference. The spatial dependence of LDOS oscillations in Eq. (10) can be evaluated by expanding the relevant quantities around each pair of EPs. Let $k_y = k_{y0}+\delta k_y$, then $\Delta k_x = \Delta k_{x0} + \sum_n \Delta k_{xn}\delta k_y^n$, $r = \sum_l \eta_l \delta k_y^l$, and $\xi_{\rm i}^{\dagger}\xi_{\rm f} = \sum_m \chi_m \delta k_y^m$. To the leading order of δk_y, the LDOS varies at long distance as

$$\begin{aligned}\delta\rho(E,x) &\simeq {\rm Re}\left[\sum_{\rm EPs}\int_E 2r/(1+|r|^2)\xi_{\rm i}^{\dagger}\xi_{\rm f}\,{\rm e}^{{\rm i}(k_x^{\rm f}-k_x^{\rm i})x}{\rm d}k_y\right]\\ &\sim \sum_{\rm EPs}|g\eta_a\chi_b c|\cos(\Delta k_{x0}x+\phi_s)x^{-(a+b+1)/c}, \quad (11)\end{aligned}$$

where $a = \min(l)$, $b = \min(m)$, $c = \min(n)$, ϕ_s is the initial phase of each pair of EPs, and

$$g = \oint_E {\rm d}k' k'^{(a+b-c+1)/c}\,{\rm e}^{{\rm i}\Delta k_{xc}k'}.$$

The decay behavior of LDOS in Eq. (11) is valid as long as $x \gg \Delta k_{x0}^{-1}$. The decay index associated with a pair of EPs is given by $(a+b+1)/c$, which is solely determined by the properties of the scattering wave function around the EPs on a given CEC.

The step edge is always along the close packed $\bar{\Gamma}$–$\bar{K}$ direction. As shown in Fig. 2(a), for Bi_2Se_3, when the Fermi energy increases, the shape of the CEC evolves from a circle ($E_1 = 0.31\varepsilon^*$), more hexagon-like ($E_2 = 0.55\varepsilon^*$), hexagon ($E_3 = 0.7\varepsilon^*$), to concave hexagon ($E_4 = 0.83\varepsilon^*$). In a wide range of energy, only a single pair of EPs exists at $(\boldsymbol{k},-\boldsymbol{k})$, so the characteristic wave vector is always equal to $2\boldsymbol{k}$ and $c = 2$. In Bi_2Te_3, the warping effect is stronger, and the power law decay behavior is more complicated. As shown in Fig. 2(b), the EPs evolve with the energy as follows: single pair of EPs $(\boldsymbol{k}_1,-\boldsymbol{k}_1)$ at $E_1 = 0.7\varepsilon^*$; multiple pairs of EPs $(\boldsymbol{k}_1,-\boldsymbol{k}_1)$, $(\boldsymbol{k}_2,-\boldsymbol{k}_3)$, and $(\boldsymbol{k}_3,-\boldsymbol{k}_2)$ at $E_2 = 1.46\varepsilon^* > E_{\rm c} \equiv 3^{1/3}\sqrt{11/9}\varepsilon^* \simeq 1.45\varepsilon^*$; two pairs of EPs $(\boldsymbol{k}_2,-\boldsymbol{k}_3)$ and $(\boldsymbol{k}_3,-\boldsymbol{k}_2)$ at $E_3 = 1.91\varepsilon^*$, as the SSs along the $\bar{\Gamma}$–$\bar{M}$ direction merge into the bulk conduction band; no EPs at all at $E_4 = 2.4\varepsilon^*$, because the SSs separate from the bulk states only in the very vicinity along the $\bar{\Gamma}$–$\bar{K}$ direction on the Fermi surface as observed in the ARPES experiment.[12] In this case, the scattering between SSs around $(\boldsymbol{k}_4,-\boldsymbol{k}_5)$ and $(\boldsymbol{k}_5,-\boldsymbol{k}_4)$ will mostly contribute to the LDOS oscillations, but they are not EPs and $c = 1$. Thus in Bi_2Te_3, the characteristic wave vector and the LDOS oscillation period critically depend on the energy of SSs via tuning the bias in the STS. In most cases we have parameter $c = 2$ except for the Fermi energy as high as E_4 ($c = 1$).

For the incoming state with wave vector $\boldsymbol{k}^{\rm i} = (k^{\rm i},\theta^{\rm i})$ and energy $\varepsilon_+(\boldsymbol{k}^{\rm i})$, the inner product of two spin wave functions is $\xi_{\rm i}^{\dagger}\xi_{\rm f} = \sin\theta^{\rm i} + {\rm i}\lambda(k^{\rm i})^3\sin(3\theta^{\rm i})\cos\theta^{\rm i}/\varepsilon_+(\boldsymbol{k}^{\rm i})$. It vanishes only for the EPs associated with zero θ, when the spins are exactly anti-parallel for the time-reversal pairs of $(\boldsymbol{k},-\boldsymbol{k})$ and $(\boldsymbol{k}_1,-\boldsymbol{k}_1)$. Since b is the lowest power for $\xi_{\rm i}^{\dagger}\xi_{\rm f}$, $b \geq 1$ for the time-reversal pairs; otherwise $b = 0$. Thus, $b = 1$ in Bi_2Se_3; while in Bi_2Te_3, $b = 1$ for the pair $(\boldsymbol{k}_1,-\boldsymbol{k}_1)$, and $b = 0$ for other pairs of EPs.

Assuming the step edge potential is $V(x) = 0$ for $x < 0$ and $V(x) = -V_0$ ($V_0 > 0$) for $x > 0$, by matching the boundary condition at the edge, we can obtain the reflection coefficient as

$$r(\theta^{\rm i}) = (-{\rm i})\frac{{\rm e}^{-{\rm i}(\theta^{\rm i}-\theta^{\rm t})/2} - \beta(\theta^{\rm i})\,{\rm e}^{{\rm i}(\theta^{\rm i}-\theta^{\rm t})/2}}{{\rm e}^{{\rm i}(\theta^{\rm i}+\theta^{\rm t})/2} + \beta(\theta^{\rm i})\,{\rm e}^{-{\rm i}(\theta^{\rm i}+\theta^{\rm t})/2}}, \quad (12)$$

where $(k^{\rm t},\theta^{\rm t})$ is the momentum of the transmitted state,

$$\beta(\theta^{\rm i}) = \frac{\varepsilon_+(\boldsymbol{k}^{\rm i})/k^{\rm i} + \lambda(k^{\rm i})^2\sin(3\theta^{\rm i})}{\varepsilon_+(\boldsymbol{k}^{\rm t})/k^{\rm t} + \lambda(k^{\rm t})^2\sin(3\theta^{\rm t})}, \quad (13)$$

$\varepsilon_+(\boldsymbol{k}^{\rm i}) = \varepsilon_+(\boldsymbol{k}^{\rm t}) - V_0$, and $\theta^{\rm t}(\theta^{\rm i}) = -\theta^{\rm t}(-\theta^{\rm i})$. Due to the constraint of the TRS, $r(\theta^{\rm i}) = -r(-\theta^{\rm i})$, and the normal reflection $r(\theta^{\rm i} = 0) = 0$, which means the absence of backscattering. The a is the lowest power for r, thus $a = 1$ for the backscattering pair of $(\boldsymbol{k},-\boldsymbol{k})$ in Bi_2Se_3 and $(\boldsymbol{k}_1,-\boldsymbol{k}_1)$ in Bi_2Te_3, and $a = 0$ for other pairs in Bi_2Te_3.

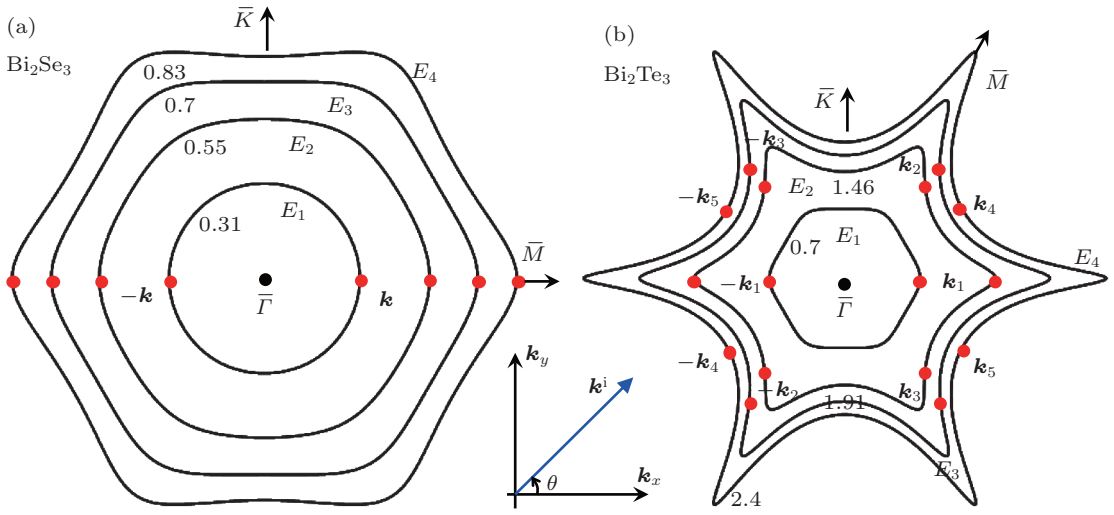


Fig. 2. Illustration of scattering off the step edge along the y direction. The LDOS oscillation is dominated by scattering between the EP pairs (red dots) on CEC. (a) The shape of CEC in Bi_2Se_3 evolves from circle, hexagon to concave hexagon as energy increases. It has a single pair of EPs at ($\boldsymbol{k}$, $-\boldsymbol{k}$), and only one type of oscillation pattern appears with different bias voltages. (b) In Bi_2Te_3, as energy increases, CEC evolves from hexagon, concave hexagon to concave hexagram, corresponding to the pair of EPs first at ($\boldsymbol{k}_1$, $-\boldsymbol{k}_1$); then at ($\boldsymbol{k}_1$, $-\boldsymbol{k}_1$), ($\boldsymbol{k}_2$, $-\boldsymbol{k}_3$), ($\boldsymbol{k}_3$, $-\boldsymbol{k}_2$); then at ($\boldsymbol{k}_2$, $-\boldsymbol{k}_3$), ($\boldsymbol{k}_3$, $-\boldsymbol{k}_2$); and finally at ($\boldsymbol{k}_4$, $-\boldsymbol{k}_5$) and ($\boldsymbol{k}_5$, $-\boldsymbol{k}_4$). Different types of oscillation patterns appear at different bias voltages.[26]

In short, the algebraical decay index is $3/2$ for $(\boldsymbol{k},-\boldsymbol{k})$ and $(\boldsymbol{k}_1,-\boldsymbol{k}_1)$ pairs, $1/2$ for $(\boldsymbol{k}_2,-\boldsymbol{k}_3)$ and $(\boldsymbol{k}_3,-\boldsymbol{k}_2)$ pairs, and 1 for $(\boldsymbol{k}_4,-\boldsymbol{k}_5)$ and $(\boldsymbol{k}_5,-\boldsymbol{k}_6)$ pairs. Therefore, the LDOS oscillations of the SSs in Bi_2Se_3 should decay as $x^{-3/2}$ in a wide range of energy (as long as $E < 0.76$ eV), much faster than $x^{-1/2}$ in 2DES.[14] On Bi_2Te_3 surfaces, as the bias increases, the LDOS oscillations decay first as $x^{-3/2}$ ($E < 0.33$ eV), then as a combination of $x^{-3/2}$ and $x^{-1/2}$, then as $x^{-1/2}$, and finally as x^{-1}.

3.2. Experiments

Kapitulnik's group performed STM and STS study on Sn- and Cd-doped Bi_2Te_3 crystals.[27] By analyzing the oscillation of LDOS near a step edge, they showed that topological SS oscillations were strongly damped compared to the conventional SSs. This is another hallmark of the severe suppression of backscattering, hence supporting the TRS protected SSs in Bi_2Te_3. An interesting observation in their experiments is the emergence of pronounced oscillations with a distinct wave vector at higher energies, which may result from a hexagonal warping of the surface band structure.

Xue's group first reported the interference fringes at the step edges on the Bi_2Se_3 surface thanks to their high quality sample.[19,26] By analyzing the decay power of standing wave oscillations across a step on Bi_2Se_3, they showed that the oscillation decays as $x^{-3/2}$, much faster than that ($x^{-1/2}$) in a 2D metal.[14] This confirms the suppression of backscattering of the topological SSs in Bi_2Se_3 due to the TRS. Such a large decay power of $-3/2$ in Bi_2Se_3 was also confirmed by Stroscio's group.[28] While in Bi_2Te_3 with a strongly warped surface band, Xue *et al*. clearly revealed the variation of the QPI decay index with the bias voltage. As shown in Table 1, as the energy of SS increases, the power law decay varies from $x^{-3/2}$ to a mixture of $x^{-3/2}$ and $x^{-1/2}$, to $x^{-1/2}$, and finally to x^{-1}. The $x^{-1/2}$ decay indicates that the suppression of backscattering due to the TRS does not necessarily lead to a spatial decay rate faster than that in the normal 2DES. As shown in Ref. [26], the agreement between the experiment of Xue's group and our theoretical prediction is surprisingly perfect.

Table 1. Index of power law decay of standing waves of SSs scattering by step edges, where ε_1 denotes the energy at which the SSs along $\bar{\Gamma}$–$\bar{M}$ begin to merge into the bulk conduction band, ε_2 denotes the energy where the SSs only exist in the very vicinity along $\bar{\Gamma}$–$\bar{K}$, and $\varepsilon_{\rm max}$ is the energy upper bound for the surface Dirac electron.

	Power decay
$0 < E < 1.45\varepsilon^*$	$x^{-3/2}$
$1.45\varepsilon^* < E < \varepsilon_1$	$x^{-3/2}, x^{-1/2}$
$\varepsilon_1 < E < \varepsilon_2$	$x^{-1/2}$
$\varepsilon_2 < E < \varepsilon_{\rm max}$	x^{-1}

4. Non-magnetic impurity

4.1. Theory

Now we switch from the 1D scattering to the 2D scattering. We first consider the interference patterns of topological SSs due to a non-magnetic impurity. The interference wave vectors of the QPI pattern can be simply understood by exploring the standing wave formation mechanism. Suppose an incident wave $\psi_{\rm i} \propto {\rm e}^{{\rm i}\boldsymbol{k}^{\rm i}\cdot\boldsymbol{r}}/\sqrt{r}$ is scattered into $\psi_{\rm f} \propto f(\theta){\rm e}^{{\rm i}\boldsymbol{k}^{\rm f}\cdot\boldsymbol{r}}/\sqrt{r}$ by the impurity potential. The resultant LDOS oscillation is

$$\delta\rho(\boldsymbol{r},\omega) \propto \sum_{\boldsymbol{k}^{\rm i},\boldsymbol{k}^{\rm f}} \frac{1}{r} f(\theta){\rm e}^{{\rm i}(\boldsymbol{k}^{\rm f}-\boldsymbol{k}^{\rm i})\cdot\boldsymbol{r}}, \tag{14}$$

with $f(\theta)$ denoting the scattering amplitude and r denoting the distance away from the impurity center. Because it is an elastic scattering, $\boldsymbol{k}^{\rm i}$ and $\boldsymbol{k}^{\rm f}$ are on the same CEC. There are various scattering directions, but most of these processes interfere destructively, contributing little to the standing waves. The interference pattern is dominated by the contribution from the pair of EPs on the CEC,[26] which resembles the Fermat's principle in optics. The characteristic scattering wavevector of the QPI pattern at a large distance in a given direction $\hat{r}$ comes from scattering between states at EPs on the Fermi surface, where the Fermi velocity is parallel to $\hat{r}$.

For the circle-like CEC shown in Fig. 3(a), the EP pair only exists at $\boldsymbol{k}$ and its time-reversal partner $-\boldsymbol{k}$. There are many such pairs, for example, $(\boldsymbol{k}_1,-\boldsymbol{k}_1)$, $(\boldsymbol{k}_2,-\boldsymbol{k}_2)$, $(\boldsymbol{k}_3,-\boldsymbol{k}_3)$, etc. Let $\boldsymbol{q}_1$ represent the backscattering vector between $\boldsymbol{k}$ and $-\boldsymbol{k}$. Obviously, there is no dominating direction of $\boldsymbol{q}_1$ in the circle case. The two states $|\boldsymbol{k},\uparrow\rangle$ and $|-\boldsymbol{k},\downarrow\rangle$, which are related by the TRS as $|-\boldsymbol{k},\downarrow\rangle = \mathscr{T}|\boldsymbol{k},\uparrow\rangle$, carry opposite spins, hence

$$\begin{aligned}\langle -\boldsymbol{k},\downarrow|\hat{U}|\boldsymbol{k},\uparrow\rangle &= -\langle \boldsymbol{k},\uparrow|\hat{U}|-\boldsymbol{k},\downarrow\rangle^* \\ &= -\langle -\boldsymbol{k},\downarrow|\hat{U}|\boldsymbol{k},\uparrow\rangle = 0. \end{aligned} \quad (15)$$

Here $\mathscr{T}$ is the time-reversal operator with $\mathscr{T}^2=-1$, and $\hat{U}$ is a TR-independent operator representing the non-magnetic scattering potential. Thus the q_1 scattering between two Krames degenerate states is forbidden, the LDOS oscillation vanishes to the leading order. Taking the next order into account, it decays algebraically as $1/r^2$. For the convex CEC shown in Fig. 3(b), there exist only two kinds of characteristic wave vectors: $\boldsymbol{q}_1$ along $\bar{\Gamma}$–$\bar{K}$ and $\boldsymbol{q}_2$ along $\bar{\Gamma}$–$\bar{M}$. Both of them connect a pair of TRS states whose scattering is prohibited, thus the LDOS oscillation decays as $1/r^2$. For the hexagon-like CEC shown in Fig. 3(c), there exist three kinds of characteristic wave vectors: $\boldsymbol{q}_1$, $\boldsymbol{q}_3$ along $\bar{\Gamma}$–$\bar{K}$ and $\boldsymbol{q}_2$ along $\bar{\Gamma}$–$\bar{M}$. Obviously, the $\boldsymbol{q}_1$ and $\boldsymbol{q}_2$ scatterings are forbidden as they connect a pair of TRS states. The $\boldsymbol{q}_3$ connects a pair of states at the EP, which dominates the QPI, and it decays as $1/r$. With the concave hexagram Fermi surface shown in Fig. 3(d), there exist only two kinds of characteristic wave vectors: $\boldsymbol{q}_1$ along $\bar{\Gamma}$–$\bar{K}$ and $\boldsymbol{q}_2$ along $\bar{\Gamma}$–$\bar{M}$. The $\boldsymbol{q}_1$ scattering is forbidden, and the $\boldsymbol{q}_2$ scattering dominates the QPI with decay index $1/r$. The characteristic wave vector and decay power of the QPI pattern are summarized in Table 2.

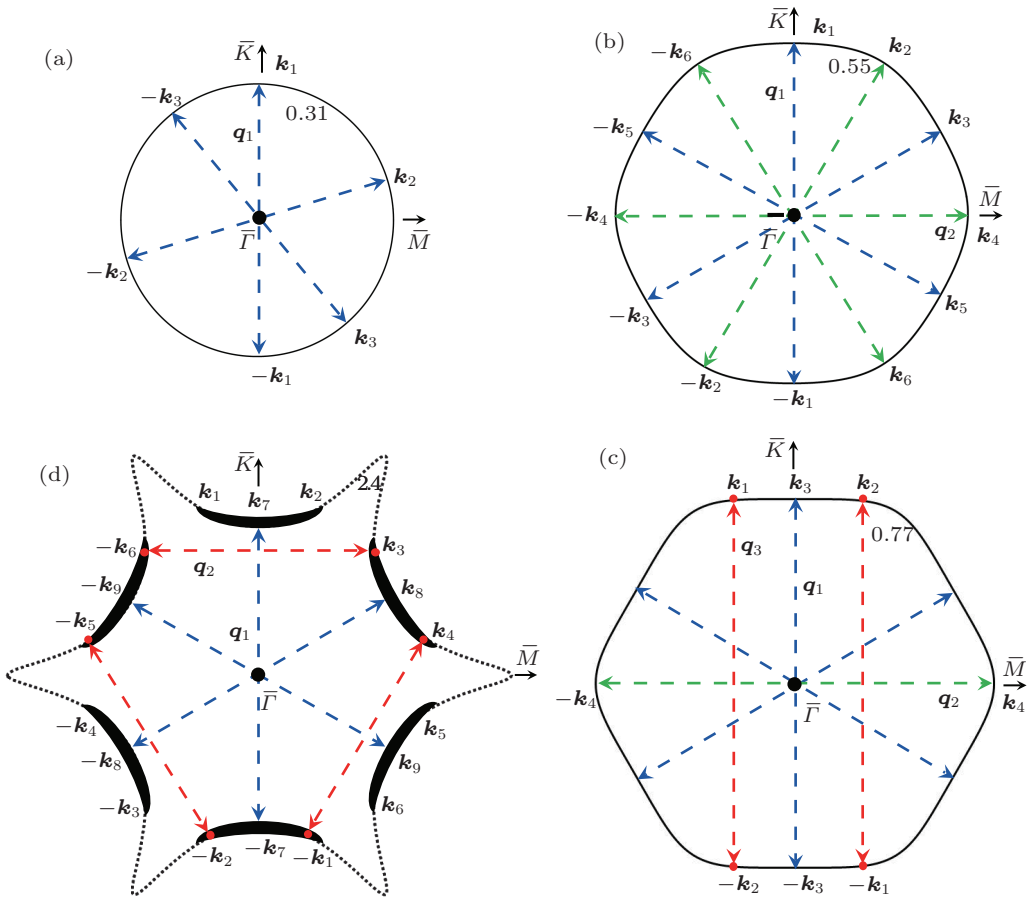


Fig. 3. Illustration of scattering geometry due to a non-magnetic impurity. The LDOS oscillation is dominated by the scattering between the pair of EPs on CEC. (a) For the CEC of circle, the pair of EPs is the SS with $\boldsymbol{k}$ and its time-reversal state with $-\boldsymbol{k}$, such as $(\boldsymbol{k}_1, -\boldsymbol{k}_1)$, $(\boldsymbol{k}_2, -\boldsymbol{k}_2)$, and $(\boldsymbol{k}_3, -\boldsymbol{k}_3)$, etc. The QPI pattern in the q-space is circular. (b) When the CEC evolves into convex, two types of forbidden characteristic wave vectors, $\boldsymbol{q}_1$ (dashed blue) and $\boldsymbol{q}_2$ (dashed green), connect the time-reversal pairs. (c) For the CEC of hexagon, $\boldsymbol{q}_1$ and $\boldsymbol{q}_2$ are forbidden, while $\boldsymbol{q}_3$ (dashed red) in the direction of $\bar{\Gamma}$–$\bar{K}$ dominates the QPI pattern. (d) For the hexagram CEC, the regions with high DOS are denoted by bold lines along the direction of $\bar{\Gamma}$–$\bar{K}$. Two types of characteristic scattering wave vectors include the forbidden $\boldsymbol{q}_1$ (dashed blue) and the allowed $\boldsymbol{q}_2$ (dashed red) which connects a pair of EPs. Thus different oscillation wave vectors appear in the FT-STS with different bias voltages.

Table 2. Characteristic wave vectors and power laws of QPI pattern for a non-magnetic impurity, where $\varepsilon_{\max}$ is the energy upper bound for the surface Dirac electron.

	Wave vector	Decay power
$0 < E < 0.4\varepsilon^*$	–	$1/r^2$
$0.4\varepsilon^* < E < 0.69\varepsilon^*$	$\bar{\Gamma}$–$\bar{K}$, $\bar{\Gamma}$–$\bar{M}$	$1/r^2$
$0.69\varepsilon^* < E < 1.45\varepsilon^*$	$\bar{\Gamma}$–$\bar{K}$	$1/r$
$1.45\varepsilon^* < E < \varepsilon_{\max}$	$\bar{\Gamma}$–$\bar{M}$	$1/r$

The scattering theory of the EPs can better interpret the experiments. In the scattering configuration for Bi_2Te_3 shown in Fig. 3(d), by numerical calculations we obtain the allowed scattering vector q_2, which varies linearly with the energy as $q_2 = 1.5\bar{k}$ (rather than $\sqrt{3}\bar{k}$[19]), where $\bar{k}$ is the length of $\bar{\Gamma}$–$\boldsymbol{k}_7$. Together with the STM data, we deduce that the Dirac velocity along $\bar{\Gamma}$–$\bar{K}$ should be $v = 4.15 \times 10^5$ m/s (instead of 4.8×10^5 m/s[19]), in agreement with ARPES result $v = 4.05 \times 10^5$ m/s.[12] In Bi_2Se_3, the CEC is circle-like up to 0.22 eV and the characteristic scattering wave vector is always along the diameter of the circle. Thus, we expect the Fourier transformation of LDOS on Bi_2Se_3 surface is ring-like.

4.2. Experiments

Yazdani's group reported their STM study of the disorder scattering of SSs on $Bi_{1-x}Sb_x$ alloy.[18] They used the energy-resolved FT-STS to draw the interference wave vectors in q space. By comparing with the spin-resolved ARPES data, a comprehensive analysis of the QPI patterns indicated that there are eight allowed scattering wave vectors, excluding those connecting states of opposite spins. With the spin-selective scattering they explicitly proved the TRS of the topological SSs in this material. More recently, STM experiments further demonstrated that the topological SSs could penetrate the barriers while maintaining their extended nature in Sb.[33]

Xue's group reported the first direct STM imaging of the standing waves on the Bi_2Te_3 (111) surface.[19] The interference fringes are caused by scattering off non-magnetic Ag atoms of the topological states. The Dirac dispersion relation of $E(k)$ of SSs was confirmed by the voltage-dependent QPI patterns. The experiment of Xue's group indicated that the backscattering of SSs is completely suppressed, which is a direct proof of the topological nature of the SSs in Bi_2Te_3. It worths mentioning that the allowed interference wave vectors in Bi_2Te_3 come from the intravalley scattering, i.e. the SSs are within the same Dirac cone; while in $Bi_{1-x}Sb_x$ alloy the scattering wave vectors are related to the intervalley scattering between the SSs in different Dirac cones.

Later, Yazdani's group reported the STM study of the QPI patterns on the surface of Ca-doped Bi_2Te_3 at several bias voltages.[20] The standing wave patterns in q space exhibited six strong peaks along the $\bar{\Gamma}$–$\bar{M}$ direction for SSs with high energies, and circular patterns with lower ones. This can be well understood on the basis of the Fermi surface shape and its associated spin texture. The warped Fermi surface in Bi_2Te_3 dominates the scattering of SSs with high energies relative to the Dirac point. In the low-energy region where the dispersion of SSs is conic, the scattering results in a simple circular pattern in the Fourier-transformed QPI. The low energy scattering pattern is also consistent with the helical spin texture of the topological SSs that still allows all scattering processes except for the direct backscattering.

5. Classical magnetic impurity

5.1. Theory

The TRS in TIs is broken by doped magnetic impurities, so in principle the backscattering process will occur, which is prohibited in the TI with non-magnetic impurities only. Here we focus on the effects of a classical magnetic impurity, which implies that the Kondo physics can be ignored.

Suppose the scattering potential of a magnetic impurity is

$$\mathscr{H}_1 = V_i \sigma^i \delta(\boldsymbol{r}) = J_i^{\text{eff}} \langle S_i \rangle \sigma^i \delta(\boldsymbol{r}), \tag{16}$$

where σ^i $(i = x, y, z)$ are the Pauli matrices denoting the electron spin, $\langle S_i \rangle$ is the expectation value of the local magnetic moment, and J_i^{eff} denotes the effective exchange coupling between electron spin and local magnetic moment. As indicated by Eq. (15), with the TRS, the backscattering is absent between a pair of TR states, $|\boldsymbol{k}, \uparrow\rangle$ and $|-\boldsymbol{k}, \downarrow\rangle$. It is thus straightforward to prove that the TRS-breaking potential such as the potential of magnetic impurities can remove such a constraint on backscattering, because

$$\mathscr{T} \sigma^i \mathscr{T}^{-1} = -\sigma^i,$$

$$\langle -\boldsymbol{k}, \downarrow | \hat{U} | \boldsymbol{k}, \uparrow \rangle \neq 0. \tag{17}$$

However, such backscattering between TR pairs can hardly be recognized in the LDOS spectra.[21] Instead of having $\delta\rho_\uparrow(\boldsymbol{q}, \omega) = \delta\rho_\downarrow(\boldsymbol{q}, \omega)$ in the non-magnetic impurity case, here we have $\delta\rho_\uparrow(\boldsymbol{q}, \omega) \approx -\delta\rho_\downarrow(\boldsymbol{q}, \omega)$. Suppose the magnetic moment of the impurity is along the z direction, then the spin-up and spin-down electrons experience opposite scattering potentials. Thus to the lowest order of perturbation theory, the scattering amplitudes of the spin-up and spin-down electrons have opposite signs, so the total interference pattern of the charge density vanishes almost everywhere

$$\begin{aligned} \delta\rho^1(\boldsymbol{q}, \omega) &\approx \int \frac{\mathrm{d}^2 k}{4\pi} \mathrm{Tr}\left[G_0(\boldsymbol{k}, \omega) \mathscr{H}_1 G_0(\boldsymbol{k} + q, \omega)\right] \\ &= \sum_i V_i \int \frac{\mathrm{d}^2 k}{4\pi} \mathrm{Tr}\left[G_0(\boldsymbol{k}, \omega) \sigma_i G_0(\boldsymbol{k} + q, \omega)\right] \\ &= 0. \end{aligned} \tag{18}$$

This argument no longer holds if higher orders of perturbation are considered. The higher order perturbations to the scattering amplitude would lead to similar results as in non-magnetic impurities.

5.2. Experiments

Recently, Madhavan's group reported first the TR violating scattering vectors in magnetically doped TI of $Bi_xFe_{2-x}Te_{3+d}$ by using FT-STM dI/dV maps.[29] Similar to the previous studies,[19] a six-fold symmetric pattern with intensity centered along the $\bar{\Gamma}$–$\bar{M}$ directions were observed above 150 meV. Remarkably, at low energies starting around 60 meV, a new set of scattering vectors centered along $\bar{\Gamma}$–$\bar{K}$ directions were found, which were not reported in the prior studies. By comparing with ARPES results, they claimed that the new scattering channels arose from the forbidden backscattering. However, at the energy 140 meV the scattering vector along $\bar{\Gamma}$–$\bar{K}$ emerged for the CEC similar to the hexagon in Fig. 3(c). The scattering vector by a non-magnetic or magnetic impurity should be along the $\bar{\Gamma}$–$\bar{K}$ direction solely due to the shape of the Fermi surface. Therefore, whether these new scattering channels arise from the forbidden backscattering or not is still in debate.

Later, Yazdani's group reported the standing wave patterns on Mn-doped Bi_2Te_3 and Bi_2Se_3.[20] The detailed Fourier analysis of the QPI patterns in q space showed that the short wavelength scatterings in different samples are similar, which are independent of whether the scattering dopant is magnetic or not, or even if the magnetic order is established. The FT-QPI pattern consists of six strong peaks along the $\bar{\Gamma}$–$\bar{M}$ directions at high energies and circular patterns at lower ones. These results strongly support that in the presence of weak magnetic impurities the backscattering between time-reversal pairs can hardly be identified in the LDOS.

Kimura's group reported the QPI pattern induced by cobalt adatoms on the Bi_2Se_3 surface by STM.[35] They found that the Co atoms are selectively adsorbed on the top of Se sites and act as strong scatter centers on the surface, generating anisotropic standing waves along $\bar{\Gamma}$–$\bar{M}$ directions. However, the long-range ferromagnetic order is absent, and the Dirac cone of SSs remains gapless. The anisotropy of the standing waves at high bias voltage is ascribed to the heavily warped CEC of unoccupied states. At low voltages, the QPI patterns due to the occupied states near Dirac cone vanishes, which suggests that the time-reversal protection of the topological SSs persists even in the presence of Co impurities.

6. Other defects

Yandani's group studied the influence of the bulk-originated disorder potential on the short-wavelength interference patterns caused by the surface impurities in $Bi_{1.95}Mn_{0.05}Te_3$.[20] They found the wave vector shift of the QPI pattern in the real-space LDOS with high and low voltages, which suggests that the surface Dirac electrons alter their wavelengths to adjust to the underlying bulk disorder potential, and are not immune to such perturbations. Whereas such fluctuations in momentum are a relatively weak perturbation to the Dirac electrons with high energies; near the Dirac point they are comparable to the average value of the momentum. The lack of well-defined momentum near the Dirac point due to the fluctuations reported is also likely to play a role in the apparent suppression of the ARPES measured signals in magnetically-doped TIs advocated recently.[36,37]

Madhavan's group used the STM and STS to investigate the effects of one-dimensional buckling on the electronic properties of Bi_2Te_3.[38] By tracking the spatial variations of the interference patterns generated by the Dirac electrons, they showed that the buckling imposes a periodic potential, which locally modulates the SS dispersion. Such a potential induces the scattering along the $\bar{\Gamma}$–$\bar{M}$ direction, which supports the absence of backscattering and well-nesting of the snowflake-like CEC.

7. Conclusion

The theoretical and experimental investigations indicate that the LDOS oscillation on the surface of TIs is generally determined by the scattering between surface states around the extremal points on the Fermi surface, either by step edges or by non-magnetic impurities. The forbidden backscattering and suppressed standing wave oscillation clearly demonstrate the 2D Dirac nature of topological surface states. The robustness of the topological surface states may have potential application in quantum computing or spintronics in the future.

References

[1] Hasan M Z and Kane C L 2010 *Rev. Mod. Phys.* **82** 3045
[2] Qi X L and Zhang S C 2011 *Rev. Mod. Phys.* **83** 1057
[3] Fu L and Kane C L 2008 *Phys. Rev. Lett.* **100** 096407
[4] Qi X L, Li R, Zang J and Zhang S C 2009 *Science* **323** 1184
[5] Li R, Wang J, Qi X L and Zhang S C 2010 *Nat. Phys.* **6** 284
[6] Fu L and Kane C L 2007 *Phys. Rev. B* **76** 045302
[7] Hsieh D, Qian D, Wray L, Xia Y, Hor Y S, Cava R J and Hasan M Z 2008 *Nature* **452** 970
[8] Hsieh D, Xia Y, Wray L, Qian D, Pal A, Dil J H, Osterwalder J, Meier F, Bihlmayer G, Kane C L, Hor Y S, Cava R J and Hasan M Z 2009 *Science* **323** 919
[9] Xia Y, Qian D, Hsieh D, Wray L, Pal A, Lin H, Bansil A, Grauer D, Hor Y S, Cava R J and Hasan M Z 2009 *Nat. Phys.* **5** 398
[10] Zhang H, Liu C X, Qi X L, Dai X, Fang Z and Zhang S C 2009 *Nat. Phys.* **5** 438
[11] Hsieh D, Xia Y, Qian D, Wray L, Dil J H, Meier F, Osterwalder J, Patthey L, Checkelsky J G, Ong N P, Fedorov A V, Lin H, Bansil A, Grauer D, Hor Y S, Cava R J and Hasan M Z 2009 *Nature* **460** 1101
[12] Chen Y L, Analytis J G, Chu J H, Liu Z K, Mo S K, Qi X L, Zhang H J, Lu D H, Dai X, Fang Z, Zhang S C, Fisher I R, Hussain Z and Shen Z X 2009 *Science* **325** 178
[13] Petersen L, Sprunger P T, Hofmann P, Læsgaard E, Briner B G, Doering M, Rust H P, Bradshaw A M, Besenbacher F and Plummer E W 1998 *Phys. Rev.* B **57** R6858
[14] Crommie M F, Lutz C P and Eigler D M 1993 *Nature* **363** 524
[15] Wittneven C, Dombrowski R, Morgenstern M and Wiesendanger R 1998 *Phys. Rev. Lett.* **81** 5616
[16] Hoffman J E, McElroy K, Lee D H, Lang K M, Eisaki H, Uchida S and Davis J C 2002 *Science* **297** 1148
[17] Rutter G M, Crain J N, Guisinger N P, Li T, First P N and Stroscio J A 2007 *Science* **317** 219

[18] Roushan P, Seo J, Parker C V, Hor Y S, Hsieh D, Qian D, Richardella A, Hasan M Z, Cava R H and Yazdani A 2009 *Nature* **460** 1106
[19] Zhang T, Cheng P, Chen X, Jia J F, Ma X, He K, Wang L, Zhang H, Dai X, Fang Z, Xie X and Xue Q K 2009 *Phys. Rev. Lett.* **103** 266803
[20] Beidenkopf H, Roushan P, Seo J, Gorman L, Drozdov I, Hor Y S, Cava R J and Yazdani A 2011 *Nat. Phys.* **7** 939
[21] Zhou X, Fang C, Tsai W F and Hu J 2009 *Phys. Rev. B* **80** 245317
[22] Lee W C, Wu C, Arovas D P and Zhang S C 2009 *Phys. Rev. B* **80** 245439
[23] Wang Q H, Wang D and Zhang F C 2010 *Phys. Rev. B* **81** 035104
[24] Guo H M and Franz M 2010 *Phys. Rev. B* **81** 041102
[25] Biswas R R and Balatsky A V 2011 *Phys. Rev. B* **83** 075439
[26] Wang J, Li W, Cheng P, Song C, Zhang T, Deng P, Chen X, Ma X, He K, Jia J F, Xue Q K and Zhu B F 2011 *Phys. Rev. B* **84** 235447
[27] Alpichshev Z, Analytis J G, Chu J H, Fisher I R, Chen Y L, Shen Z X, Fang A and Kapitulnik A 2010 *Phys. Rev. Lett.* **104** 016401
[28] Zhang T, Levy N, Ha J, Kuk Y and Stroscio J A 2013 *Phys. Rev. B* **87** 115410
[29] Okada Y, Dhital C, Zhou W, Huemiller E D, Lin H, Basak S, Bansil A, Huang Y B, Ding H, Wang Z, Wilson S D and Madhavan V 2011 *Phys. Rev. Lett.* **106** 206805
[30] Fu L 2009 *Phys. Rev. Lett.* **103** 266801
[31] Huang L T and Zhu B F 2012 *Proceedings of the* 31*st International Conference on the Physics of Semiconductors*, 2012, July 29–August 4, Zurich, Switzerland
[32] Kuroda K, Arita M, Miyamoto K, Ye M, Jiang J, Kimura A, Krasovskii E E, Chulkov E V, Iwasawa H, Okuda T, Shimada K, Ueda Y, Namatame H and Taniguchi M 2010 *Phys. Rev. Lett.* **105** 076802
[33] Seo J, Roushan P, Beidenkopf H, Hor Y S, Cava R J and Yazdani A 2010 *Nature* **466** 343
[34] Roth L M, Zeiger H J and Kaplan T A 1966 *Phys. Rev.* **149** 519
[35] Ye M, Eremeev S V, Kuroda K, Krasovskii E E, Chulkov E V, Takeda Y, Saitoh Y, Okamoto K, Zhu S Y, Miyamoto K, Arita M, Nakatake M, Okuda T, Ueda Y, Shimada K, Namatame H, Taniguchi M and Kimura A 2012 *Phys. Rev. B* **85** 205317
[36] Chen Y L, Chu J H, Analytis J G, Liu Z K, Igarashi K, Kuo H H, Qi X L, Mo S K, Moore R G, Lu D H, Hashimoto M, Sasagawa T, Zhang S C, Fisher I R Hussain Z and Shen Z X 2010 *Science* **329** 659
[37] Wray L A, Xu S Y, Xia Y, Hsieh D, Fedorov A V, Hor Y S, Cava R J, Bansil A, Lin H and Hasan M Z 2010 *Nat. Phys.* **7** 32
[38] Okada Y, Zhou W, Walkup D, Dhital C, Wilson S D and Madhavan V 2012 *Nature Commun.* **3** 1158